Biointerface Research in Applied Chemistry
Open-Access Journal (ISSN: 2069-5837)

Article
Volume 13, Issue 5, 2023, 421
https://doi.org/10.33263/BRIAC135.421

Carbon Dioxide Uptake by a Polonium-Doped Fullerene: Computational Analyses

Kun Harismah [1], Ali Hassan [2], Maadh Fawzi Nassar [3,4], Omar Talal Hamid [5], Hasan Zandi [6,*]

1 Department of Chemical Engineering, Faculty of Engineering, Universitas Muhammadiyah Surakarta, Surakarta, Indonesia; kun.harismah@ums.ac.id (K.H.);
2 Department of Medical Instruments Engineering Techniques, Bilad Alrafidain University College, Diyala Junction, Baqubah, Diyala, Iraq; alihabeel@hotmail.com (A.H.);
3 Integrated Chemical BioPhysics Research, Faculty of Science, Universiti Putra Malaysia, 43400 UPM Serdang, Selangor, Malaysia; nassarmaadh@gmail.com (M.F.N.);
4 Department of Chemistry, Faculty of Science, Universiti Putra Malaysia, 43400 UPM Serdang, Selangor, Malaysia; nassarmaadh@gmail.com (M.F.N.);
5 Department of Oil and Gas Refining Engineering, Al-Turath University College, Baghdad, Iraq; omar.talal@turath.edu.iq (O.T.H.);
6 Department of Chemistry, Faculty of Science, University of Qom, Qom, Iran; h.zandi.dr@gmail.com (H.Z.);
* Correspondence: h.zandi.dr@gmail.com (H.Z.);

Scopus Author ID 14122606900
Received: 17.06.2022; Accepted: 18.07.2022; Published: 22.11.2022

Abstract: The idea of carbon dioxide (CO_2) uptake by a polonium-doped fullerene (PoF) was investigated in this work by performing computational analyses of structural and electronic features. To this aim, the singular models of CO_2 and PoF (polonium-carbon-19) were optimized, and they participated in interactions to reach the formation of CO_2@PoF bimolecular complexes. Accordingly, two models were obtained, C1 and C2, with two and one interaction, respectively. Analyses of adsorption strength indicated higher stability for C1 compared to C2. Further analyses of electronic molecular orbital features revealed a dominant role of PoF for adsorbing the CO_2 substance by movement of whole frontier molecular orbitals patterns to the PoF part of the complex. In this regard, the models were also observed to be detectable by variations of such electronic molecular orbitals features. Indeed, energy levels of the highest occupied and the lowest unoccupied molecular orbitals (HOMO and LUMO) and these levels' energy distance could help approach the diagnosis. Consequently, the idea of CO_2 uptake by PoF was confirmed by the evaluated structural and electronic features of models in singular and bimolecular modes proposing CO_2@PoF complexes for further investigations of CO_2-based devices.

Keywords: fullerene; doped nanostructure; carbon dioxide; gas adsorption; DFT.

1. Introduction

The innovation of nanostructures and technology encouraged researchers to work on the exploration of various aspects of these novel concepts in all fields of science and engineering [1-4]. Accordingly, several geometrical shapes of nanostructures were found to specify their technological features and characters [5-8]. From the first days of such remarkable innovation, the surface area of nanostructures has been found suitable for adsorbing other substances in terms of bimolecular or multimolecular complex formations [9-12]. Indeed, this was an important achievement because of the dominant role of the adsorption process in several fields, such as filtration, separation, recognition, and even drug delivery functions [13-16]. To

this aim, several efforts have been dedicated to recognizing such featured surfaces for working in specific processes such as gas uptake and adsorption [17-20]. Further investigations indicated that the heteroatomic nanostructures could work better than the pure nanostructures to play efficient adsorbents' roles [21-24]. Atomic dopants, especially those metal atoms with vacant orbitals, could provide an activated site of interactions for the nanostructures to participate in more efficient adsorption [25-28]. In this regard, several methodologies have been developed to recognize such characteristic features for the complicated systems of nanostructures. The computational analyses were seen as suitable for approaching the purposes by revealing details insights into interactions [29-32]. Indeed, several attempts have always been dedicated to developing novel techniques of recognition of the features of complicated systems in accordance with the innovation of their applications for various fields of sciences and engineering [33-36].

Fullerene is a spherical cage of carbon nanostructures, which has been recognized prior to the well-known carbon nanotube (CNT) [37-40]. Further investigations indicated the characteristic roles of fullerene for approaching various purposes of the development of nanostructures applications [41]. To this aim, several atomic compositions of fullerenes have been introduced up to now based on the number of carbon atoms and their doped models [42]. Carbon-60 fullerene was indeed the first introduced fullerene nanostructure, and other carbon-n (n with different numbers) were introduced next [43]. For running the molecular calculations to know the details of adsorption and interaction systems, carbon-20 was found to be a suitable model [44]. Accordingly, a model of carbon-20 fullerene with polonium (Po) atomic dopant (PoF) was investigated in this work for conducting the carbon dioxide (CO_2) uptake (Figures 1 and 2). It is known that the existence of CO_2 is crucial for the environment and living systems, but the over-exhaustion of this gas could lead to different pollution and global warming issues [45-47]. CO_2 is among the greenhouse gases, with a majority of production/consumption among all other gases [48]. Therefore, developing novel CO_2 uptake processes and devices is important for maintaining the general health level. It has been seen as an important issue for the living systems, especially for human life [49-52].

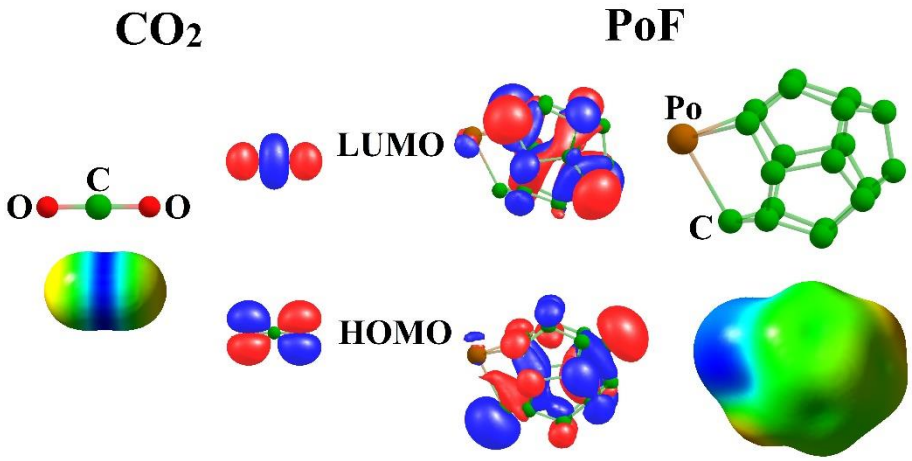

Figure 1. CO_2 and PoF singular models, HOMO-LUMO patterns, and ESP surfaces.

Within the current research work, quantum density functional theory (DFT) computational analyses were done to investigate the processes of CO_2 uptake by a PoF nanostructure. To approach the goal, optimization calculations and molecular/atomic feature evaluations were performed to provide the required information. As shown in Figures 1 and 2, the singular (CO_2 and PoF) and bimolecular (CO_2@PoF) models were exhibited. Accordingly,

their corresponding quantitative descriptors were summarized in Tables 1 and 2, besides further electronic representations of Figure 3. This work's main goal was to recognize CO_2 uptake by a PoF model and learn details of such processes for developing new CO_2-based devices. The topic of CO_2 detection and removal has been seen as important, especially with the problems of global warming and greenhouse gas exhaustion, and several works have been currently focusing on this topic with various methodologies [53-56].

2. Materials and Methods

The Computational analyses of this work were done by performing quantum DFT calculations using the B3LYP exchange-correlation functional, the 6-31G* standard basis set for C and O atoms, and the def2-SVP basis set for Po atom as all implemented in the Gaussian program [57]. First, the individual models of CO_2 and PoF (Figure 1) were optimized to prepare the input materials for the adsorption process. Next, the bimolecular models of CO_2@PoF, C1, and C2 (Figure 2) were stabilized by involving the already optimized singular models in new optimization calculations. The optimized models were obtained to evaluate their structural and electronic descriptors in this step. Features of the quantum theory of atoms in molecules (QTAIM) [58] were evaluated (Table 1) to know the details of interactions for the CO_2@PoF bimolecular models. Next, energy features for the whole structure and molecular orbitals were evaluated (Table 2) to know the details of adsorption strength and the corresponding electronic variations. Additionally, distribution patterns of the highest occupied molecular orbital (HOMO) and the lowest unoccupied molecular orbital (LUMO) were exhibited in each of Figures 1 and 2 besides the evaluated electrostatic potential (ESP) surfaces. Additionally, diagrams of the density of states (DOS) were illustrated (Figure 3) for the models to show molecular orbitals variations before/after HOMO and LUMO levels. Consequently, the required quantitative and qualitative information was prepared for describing the models of this work through the benefits of performing computational analyses of complicated systems [59-63].

Table 1. The evaluated QTAIM features of CO_2@PoF bimolecular models.[1]

Model	Interaction	Distance (Å)	Rho (au)	Del2-Rho (au)	H (au)
C1	O…Po	3.38	0.082	0.027	-0.083
	C…C	3.04	0.011	0.033	-0.015
C2	O…Po	3.29	0.086	0.028	-0.091

[1] The models are shown in Figures 1 and 2.

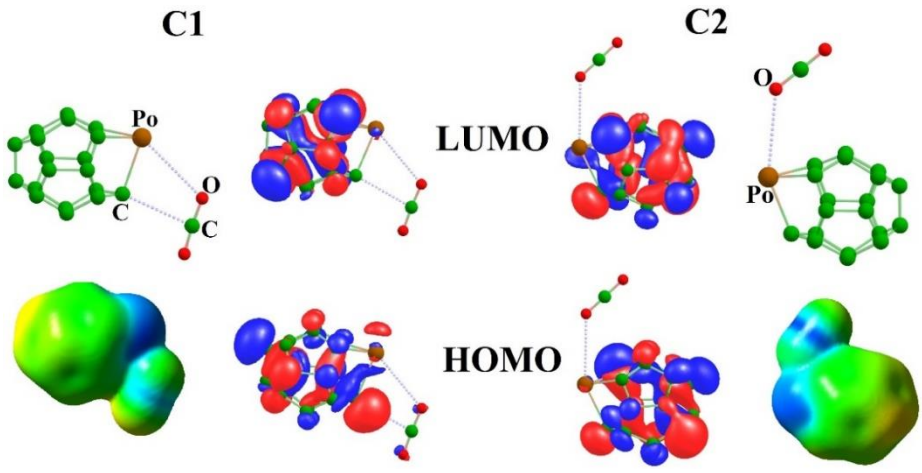

Figure 2. C1 and C2 CO_2@PoF bimolecular models, HOMO-LUMO patterns, and ESP surfaces.

3. Results and Discussion

The parental models of this work were CO_2 and PoF molecules, in which their possible combinations were investigated to approach the idea of CO_2 uptake by a PoF surface. As shown in Figure 1, the models and their HOMO-LUMO patterns and ESP surfaces were exhibited. PoF stands for a polonium-doped carbon-20 fullerene yielding a composed polonium-carbon-19 structure. Accordingly, the ESP surfaces showed positive-charge blue at the polonium atom region, which repealed this atom's dominant role in interacting with the CO_2 substance. Both singular models were optimized to obtain their stabilized geometries for their preparation for participating in interactions. Next, various initial configurations of complexes of CO_2 and PoF were examined up to reaching the finalized CO_2@PoF geometries as a result of two C1 and C2 configurations. The final possible biomolecular models are shown in Figure 2, besides their HOMO-LUMO patterns and ESP surfaces. Comparing the HOMO-LUMO pattern of singular and bimolecular models could show the movement of all molecular orbital patterns of CO_2 to PoF in both C1 and C2 bimolecular structures. These models were finalized by examining all possibilities and recognizing the corresponding geometries. Accordingly, the models were stabilized in two configurations, in which the orientation of O=C=O was relaxed parallel to the orientation of the C-Po bond of PoF in C1, whereas it was located between two C-Po bonds of PoF in C2. However, the electronic features showed movements of molecular orbitals patterns to the PoF part. For analyzing details of interactions, the QTAIM features were evaluated in Table 1. Based on the obtained results, two interactions, O…Po and C…C, were observed for the formation of C1, and one interaction, O…Po, was observed for the formation of C2. Additionally, their evaluated features, Rho (total electron density), Del2-Rho (Laplacian of electron density), and H (energy of electron density), showed meaningful strengths for the involved interactions. Since C1 involved two interactions, its strength could be expected to be higher than C2. In this part, the models were recognized by their interactions for formations of C1 and C2 CO_2@PoF bimolecular complexes. It should be mentioned that physical types of interactions were observed for the interacting models making the possibility of conducting a reversible process of gas adsorption.

Table 2. The evaluated energy features of singular and bimolecular models.[1]

Model	E_{Ads} (kcal/mol)	HOMO (eV)	LUMO (eV)	E_{Gap} (eV)	E_{Fermi} (eV)	CH (eV)	CS (eV^{-1})
C1	-19.18	-4.75	-2.99	1.77	-3.87	0.88	1.13
C2	-5.77	-4.63	-2.90	1.73	-3.76	0.86	1.16
CO_2	n/a	-10.07	0.81	10.88	-4.63	5.44	0.18
PoF	n/a	-4.64	-2.94	1.69	-3.79	0.85	1.18

[1]The models are shown in Figures 1 and 2.

The energy features of the investigated singular and bimolecular models are summarized in Table 2. To make a quantitative analysis of the adsorption strength, values of E_{Ads} (energy of adsorption) were evaluated for C1 and C2 by measuring energy differences between CO_2@PoF and each of the CO_2 and PoF models. In this regard, the calculated energies showed a higher strength of C1 (E_{Ads} = -19.18 kcal/mol) in comparison with C2 (E_{Ads} = -5.77 kcal/mol). Returning to the evaluated QTAIM features, C1 contributed to two interactions, and C2 contributed to one interaction. Accordingly, a higher adsorption strength was observed for C1 compared to C2. It is noted that both C1 and C2 CO_2@PoF bimolecular models were in a reasonable strength level of adsorption. Consequently, the idea of CO_2 uptake by PoF was confirmed in this step.

Further models were analyzed by their evaluated values of molecular orbitals and related features. It is known that HOMO stands for the electron-full level of molecular orbitals, and LUMO stands for the electron-vacant level of molecular orbitals. In this regard, variations of these levels could be found by analyzing the energy levels and the evaluated distribution patterns. It was observed in Figure 2 that the patterns were moved to the PoF part and the ESP surfaces showed connectivity of such electron surfaces for the formation of a complex structure. Accordingly, the PoF model was realized to be suitable for the adsorption of CO_2 by collecting all the molecular orbital patterns at the PoF part in both C1 and C2 CO_2@PoF bimolecular complexes. Examining the values of HOMO and LUMO (Table 2) could show the impact of complex formations on the electronic molecular orbital features. In agreement with the evaluated patterns, the values of complexes were closer to the values of singular PoF than those of singular CO_2. The illustrated diagrams of DOS (Figure 3) could also approve such variations, in which HOMO and LUMO levels were changed besides other levels before/after these. Accordingly, a diagnosis process could be detectable for the formation of each of the CO_2@PoF bimolecular complex models. In this regard, a sensor function could be assumed for the investigated models to approach the purpose of detecting adsorbed gas. The values of E_{Gap} (energy gap) indicated the energy distances of the frontier HOMO and LUMO levels, and the average value of this distance was assigned by the value of E_{Fermi} (energy of Fermi level). Next, the evaluated values of CH and CS (chemical hardness and softness) showed the benefits of such CO_2@PoF complex formations for further applications of adsorbed CO_2.

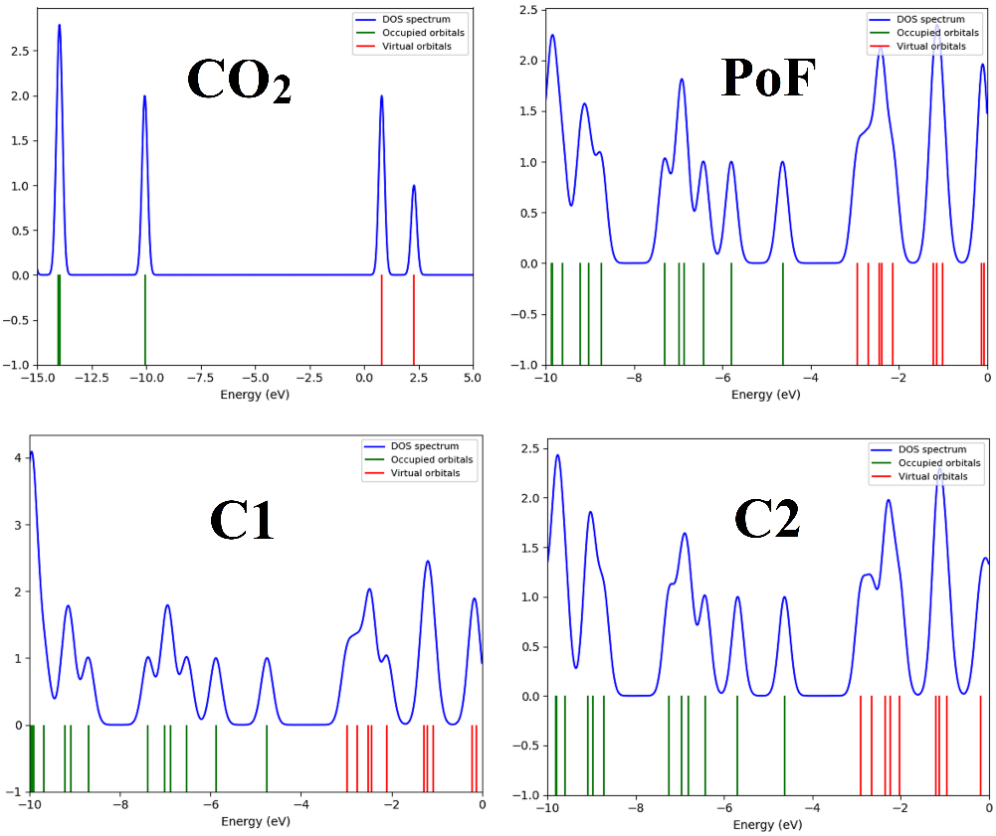

Figure 3. DOS diagrams of the models.

4. Conclusions

The idea of CO_2 uptake by PoF was investigated in this work based on the computational analysis results. After optimizing the singular CO_2 and PoF structures, they were combined to obtain two CO_2@PoF bimolecular models; C1 and C2. The results of QTAIM

analyses indicated the existence of two interactions in C1 and one in C2, and the adsorption strength of C1 was higher than C2. The evaluated features of electronic molecular orbitals indicated variations of HOMO-LUMO levels in both quantity and quality. Such features of complexes were closer to the singular PoF model than the singular CO_2 model. Next, examining the distribution patterns and DOS diagrams affirmed such achievement. Consequently, the models of CO_2@PoF were obtained, and their structural stabilities and electronic features were analyzed to approach the affirmation of CO_2 uptake by PoF for further developments of CO_2-based devices.

Funding

This research received no external funding.

Acknowledgments

This research has no acknowledgment.

Conflicts of Interest

The authors declare no conflict of interest.

References

1. Sahoo, M.; Vishwakarma, S.; Panigrahi, C.; Kumar, J. Nanotechnology: current applications and future scope in food. *Food Frontiers* **2021,** *2,* 3–22, https://doi.org/10.1002/fft2.58.
2. Khalili, A.; Dehno Khalaji, A.; Mokhtari, A.; Keyvanfard, M. Synthesis, characterization, and methyl green removal of epichlorohydrin crosslinked schiff base chitosan/Fe_2O_3 nanocomposite. *Progress in Chemical and Biochemical Research* **2021,** *4,* 392–402, https://doi.org/10.22034/pcbr.2021.290770.1192.
3. Kreydie, S.; Al-Abdaly, B. Synthesis, characterization and evaluation of inhibition corrosion of bacterial cellulose/metal oxides nanocomposites. *Eurasian Chemical Communications* **2021,** *3,* 706–714, https://doi.org/10.22034/ecc.2021.299439.1216.
4. Hatami, A.; Heydarinasab, A.; Akbarzadehkhiyavi, A.; Pajoum Shariati, F. An introduction to nanotechnology and drug delivery. *Chemical Methodologies* **2021,** *5,* 153–165, https://doi.org/10.22034/chemm.2021.121496.
5. Dehno Khalaji, A.; Machek, P.; Jarosova, M. α-Fe_2O_3 nanoparticles: synthesis, characterization, magnetic properties and photocatalytic degradation of methyl orange. *Advanced Journal of Chemistry-Section A* **2021,** *4,* 317–326, https://doi.org/10.22034/ajca.2021.292396.1268.
6. Jabbari, R.; Ghasemi, N. Investigating methylene blue dye adsorption isotherms using silver nano particles provided by aqueous extract of tragopogon buphthalmoides. *Chemical Methodologies* **2021,** *5,* 21–29, https://doi.org/10.22034/chemm.2021.118446.
7. Bashandeh, Z.; Dehno Khalaji, A. Effective removal of methyl green from aqueous solution using epichlorohydrine cross-linked chitosan. *Advanced Journal of Chemistry-Section A* **2021,** *4,* 270–277, https://doi.org/10.22034/ajca.2021.285520.1259.
8. Khakyzadeh, V.; Rezaei-Vahidian, H.; Sediqi, S.; Azimi, S.; Karimi-Nami, R. Programming adsorptive removal of organic azo dye from aqueous media using magnetic carbon nano-composite. *Chemical Methodologies* **2021,** *5,* 324–330, https://doi.org/10.22034/chemm.2021.131300.
9. Yaraghi, A.; Ozkendir, O.M.; Mirzaei, M. DFT studies of 5-fluorouracil tautomers on a silicon graphene nanosheet. *Superlattices and Microstructures* **2015,** *85,* 784–788, https://doi.org/10.1016/j.spmi.2015.05.053.
10. Shahamatpour, M.; Tabatabaee Ghomsheh, S.; Maghsoudi, S.; Azizi, S. Fenton processes, adsorption and nano filtration in industrial wastewater treatment. *Progress in Chemical and Biochemical Research* **2021,** *4,* 32–43, https://doi.org/10.22034/pcbr.2021.118152.

11. Sanati, M.; Dehno Khalaji, A.; Mokhtari, A.; Keyvanfard, M. Fast removal of methyl green from aqueous solution by adsorption onto new modified chitosan Schiff base. *Progress in Chemical and Biochemical Research* **2021,** *4,* 319–330, https://doi.org/10.22034/pcbr.2021.285530.1186.
12. Nabi Bidhendi, G.; Mehrdadi, N.; Firouzbakhsh, M. Removal of lead from wastewater by iron–benzenetricarboxylate metal-organic frameworks. *Chemical Methodologies* **2021,** *5,* 271–284, https://doi.org/10.22034/chemm.2021.130208.
13. Belhadri, M.; Mokhtar, A.; Bengueddach, A.; Sassi, M. Efficient adsorbent based on bentonite functionalized with 3-aminopropyltriethoxysilane for dyes removal from aqueous solutions. *Eurasian Chemical Communications* **2021,** *3,* 881–892, https://doi.org/10.22034/ecc.2021.305858.1240.
14. Hanafizadeh, P.; Karimi, A.; Taklifi, A.; Hojati, A. Experimental investigation of two-phase water–oil flow pressure drop in inclined pipes. *Experimental Thermal and Fluid Science* **2016,** *74,* 169–180, https://doi.org/10.1016/j.expthermflusci.2015.11.024.
15. Tavoosi, F.; Movahedi, M.; Rasouli, N. Preparation and comparison of two different nanocomposite kinds based on MgZnAl-layered double hydroxide for simultaneous removal of cationic and anionic dyes, *Advanced Journal of Chemistry-Section A* **2021,** *4,* 32–41, https://doi.org/10.22034/ajca.2021.253006.1217.
16. Mirnezami, S.; Zare Kazemabadi, F.; Heydarinasab, A. Sulfur production by hydrogen sulfide biological removal from pollutants. *Progress in Chemical and Biochemical Research* **2021,** *4,* 191–206, https://doi.org/10.22034/pcbr.2021.277907.1182.
17. Zare, B.; Ameri, E.; Sadeghi, M. Dehydration of natural gas using polyether sulfone (PES) membrane and its nanocomposite with silica particles and nitrogen sweeping gas. *Chemical Methodologies* **2021,** *5,* 308–316, https://doi.org/10.22034/chemm.2021.131096.
18. Torabi, Z.; Saeida Ardekani, S.; Hataminasab, S. New model of professional competence of managers of hotels, oil, gas and energy industries toward sustainable development. *Advanced Journal of Chemistry-Section A* **2021,** *4,* 231–243, https://doi.org/10.22034/ajca.2021.277904.1247.
19. Ariaei, S.; Sakhaeinia, H.; Heydarinasab, A.; Shokouhi, M. CO and NO selective adsorption by a $C_{16}Mg_8O_8$ nanocage: a DFT Study. *Main Group Chemistry* **2021,** *20,* 489–499, https://doi.org/10.3233/MGC-210060.
20. Harismah, K.; Nayini, M.M.; Montazeri, S.; Ariaei, S.; Nouraliei, M. DFT investigation of SiO_2 nanotube for adsorption of methyl-and propyl-paraben. *Main Group Chemistry* **2021,** *20,* 355–363, https://doi.org/10.3233/mgc-210052.
21. Ghiasifar, M.; Hosseinnejad, T.; Ahangar, A. Copper catalyzed cycloaddition reaction of azidomethyl benzene with 2,2-Di(prop-2-yn-1-yl)propane-1,3-diol: DFT and QTAIM investigation. *Progress in Chemical and Biochemical Research* **2022,** *5,* 1–20, https://doi.org/10.22034/pcbr.2022.319090.1203.
22. Abd AL-Zahra, A.; Al-Sammarraie, A. Hydrothermal synthesis and characterization of zinc sulfide nanoparticles. *Eurasian Chemical Communications* **2021,** *3,* 606–613, https://doi.org/10.22034/ecc.2021.293399.1196.
23. Baghernejad, B.; Nazari, L. Synthesis of indeno [1,2-b] pyridine derivatives in the precense of Nano CeO_2/ZnO. *Eurasian Chemical Communications.* **2021,** *3,* 319–326, https://doi.org/10.22034/ecc.2021.277002.1145.
24. Asgari Bajgirani, M. Application of Ziegler-Nata catalysts in the synthesis of polyolefin. *Progress in Chemical and Biochemical Research* **2021,** *4,* 20–31, https://doi.org/10.22034/pcbr.2021.118046.
25. Kazemi, F.; Zamani, H.; Abedi, M.; Ebrahimi, M. Photodegradation of tramadol using α-Fe_2O_3 nanoparticles/ 12-tungstosilicic acid as an efficient photocatalyst in water sample employing box-behnken design. *Chemical Methodologies* **2021,** *5,* 522–533, https://doi.org/10.22034/chemm.2021.138835.
26. Pari, A.A.; Yousefi, M.; Samadi, S.; Allahgholi Ghasri, M.R.; Torbati, M.B. Structural analysis of an iron-assisted carbon monolayer for delivery of 2-thiouracil. *Main Group Chemistry* **2021,** *20,* 653–661, https://doi.org/10.3233/mgc-210079.
27. Khodadadi, A.; Talebtash, M.R. Investigation and synthesis of Fe doped Al2O3 nanoparticles by Co-precipitation and sol gel methods. *Asian Journal of Nanosciences and Materials* **2022,** *5,* 36–47, https://doi.org/10.26655/AJNANOMAT.2022.1.4.
28. Karimi, A.; Hekmat-Ara, A.; Zare, A.; Barzegar, M.; Khanivar, R.; Sadeghi-Takallo, M. Producing, characterizing and utilizing a novel magnetic catalyst to promote construction of N,N′-alkylidene bisamides. *Eurasian Chemical Communications* **2021,** *3,* 360–368, https://doi.org/10.22034/ecc.2021.277415.1149.
29. Anafcheh, M. A comparison between density functional theory calculations and the additive schemes of polarizabilities of the Li-F-decorated BN cages. *Journal of Applied Organometallic Chemistry* **2021,** *1,* 125–133, https://doi.org/10.22034/jaoc.2021.292384.1027.

30. Dhonnar, S.; Sadgir, N.; Adole, V.; Jagdale, B. Molecular structure, FT-IR spectra, MEP and HOMO-LUMO investigation of 2-(4-Fluorophenyl)-5-phenyl-1, 3,4-oxadiazole using DFT theory calculations. *Advanced Journal of Chemistry-Section A* **2021,** *4,* 220–230, https://doi.org/10.22034/ajca.2021.283003.1254.
31. Darougari, H.; Rezaei-Sameti, M. The drug delivery appraisal of Cu and Ni decorated B12N12 nanocage for an 8-hydroxyquinoline drug: A DFT and TD-DFT computational study. *Asian Journal of Nanosciences and Materials* **2022,** *5,* 196–210, https://doi.org/10.26655/AJNANOMAT.2022.3.3.
32. Adole, V. Synthesis, antibacterial, antifungal and DFT studies on structural, electronic and chemical reactivity of (E)-7-((1H-Indol-3-yl)methylene)-1,2,6,7-tetrahydro-8H-indeno[5,4-b]furan-8-one. *Advanced Journal of Chemistry-Section A* **2021,** *4,* 175–187, https://doi.org/10.22034/ajca.2021.278047.1250.
33. Wikantyasning, E.R.; Mutmainnah, M.; Cholisoh, Z.; Hairunisa, I.; Bakar, M.F.A.; Da'i, M. Preparation of hydrogel nanocomposite containing gold nanoparticles with unique swelling/deswelling properties. *Rasayan Journal of Chemistry* **2019,** *12,* 1857–1863, https://doi.org/10.31788/rjc.2019.1245209.
34. Da'i, M.; Suhendi, A.; Meiyanto, E.; Jenie, U.A.; Kawaichi, M. Apoptosis induction effect of curcumin and its analogs pentagamavunon-0 and pentagamavunon-1 on cancer cell lines. *Asian Journal of Pharmaceutical and Clinical Research* **2017,** *10,* 373–376, https://doi.org/10.22159/ajpcr.2017.v10i3.16311.
35. Şahin, K.E.; Baglan Uzunget, S.; Keskinruzgar, A. Elastic properties of the aorta are affected in young patients with sleep bruxism. *International Journal of Scientific Research in Dental and Medical Sciences* **2021**, *3*, 171–178, https://doi.org/10.30485/ijsrdms.2021.315608.1216.
36. Jamali, S.; Basturk, F.B.; Das, M.; de Oliveira Pinto, R. The effect of passive ultrasonic irrigation in comparison with other techniques on removing calcium hydroxide from root canals: a systematic review. *International Journal of Scientific Research in Dental and Medical Sciences* **2019,** *1,* 80–83, https://doi.org/10.30485/ijsrdms.2019.192766.1009.
37. Liu, J.; Qiu, L.; Shao, S. Emerging electronic applications of fullerene derivatives: an era beyond OPV. *Journal of Materials Chemistry C* **2021,** *9,* 16143–16163, https://doi.org/10.1039/d1tc04038c.
38. Heredia, D.A.; Durantini, A.M.; Durantini, J.E.; Durantini, E.N. Fullerene C60 derivatives as antimicrobial photodynamic agents. *Journal of Photochemistry and Photobiology C: Photochemistry Reviews* **2022,** *51*, 100471, https://doi.org/10.1016/j.jphotochemrev.2021.100471.
39. Maji, S.; Shrestha, L.K.; Ariga, K. Nanoarchitectonics for hierarchical fullerene nanomaterials. *Nanomaterials* **2021,** *11,* 2146, https://doi.org/10.3390/nano11082146.
40. Shabani, M.; Ghiasi, R.; Zare, K.; Fazaeli, R. The interaction between carboplatin anticancer drug and B12N12 nano-cluster: a computational investigation. *Main Group Chemistry* **2021,** *20,* 345–354, https://doi.org/10.3233/mgc-210051.
41. Kumar, P.; Namboodiri, V.V.; Joshi, G.; Mehta, K.P. Fabrication and applications of fullerene-based metal nanocomposites: a review. *Journal of Materials Research* **2021,** *36,* 114–128, https://doi.org/10.1557/s43578-020-00094-1.
42. Muz, İ.; Göktaş, F.; Kurban, M. A density functional theory study on favipiravir drug interaction with BN-doped C60 heterofullerene. *Physica E: Low-dimensional Systems and Nanostructures* **2022,** *135,* 114950, https://doi.org/10.1016/j.physe.2021.114950.
43. Ferreira, R.A.; dos Santos, J.R.; Falleiros, J.M.; da Silva, E.L.; dos Santos, J.D. Functionalization of fullerene isomers [60, 70, 80 and 82] with R-thiazolidinethione: a DFT study. *Chemical Physics Letters* **2021,** *769,* 138421, https://doi.org/10.1016/j.cplett.2021.138421.
44. Kosar, N.; Tahir, H.; Ayub, K.; Gilani, M.A.; Imran, M.; Mahmood ,T. Remarkable nonlinear optical response of Mn@C20 (M= Na & K and n= 1–6); a DFT outcome. *Materials Science in Semiconductor Processing* **2022,** *138,* 106269, https://doi.org/10.1016/j.mssp.2021.106269.
45. Park, J.H.; Yang, J.; Kim, D.; Gim, H.; Choi, W.Y.; Lee, J.W. Review of recent technologies for transforming carbon dioxide to carbon materials. *Chemical Engineering Journal* **2022,** *427,* 130980, https://doi.org/10.1016/j.cej.2021.130980.
46. Rosa, L.; Sanchez, D.L.; Mazzotti, M. Assessment of carbon dioxide removal potential via BECCS in a carbon-neutral Europe. *Energy & Environmental Science* **2021,** *14,* 3086–3097, https://doi.org/10.1039/d1ee00642h.
47. Terlouw, T.; Bauer, C.; Rosa, L.; Mazzotti, M. Life cycle assessment of carbon dioxide removal technologies: a critical review. *Energy & Environmental Science* **2021,** *14,* 1701–1721, https://doi.org/10.1039/d0ee03757e.
48. Nong, D.; Simshauser, P.; Nguyen, D.B. Greenhouse gas emissions vs CO2 emissions: comparative analysis of a global carbon tax. *Applied Energy* **2021,** *298,* 117223, https://doi.org/10.1016/j.apenergy.2021.117223.

49. Jamali, S.; Ahmadi, F.; Mahdavi-Mazdeh, M.; Tavoosi, A. The relationship between serum uric acid level and pulmonary artery hypertension in patients with chronic renal failure. *International Journal of Scientific Research in Dental and Medical Sciences* **2019,** *1,* 23–25, https://doi.org/10.30485/ijsrdms.2019.89759.
50. Kumar, A.; Gupte, B.; Shangloo, P. Effect of nicotine smoke on genitourinary organs of male albino rats: an experimental study. *International Journal of Scientific Research in Dental and Medical Sciences* **2021,** *3,* 141–146, https://doi.org/10.30485/ijsrdms.2021.296503.1177.
51. Jerin, T.; Sharmin, N.; Raihan, S. Silico functional annotation and molecular characterization of an uncharacterized protein MBO_502153 of mycobacterium tuberculosis variant bovis. *International Journal of Scientific Research in Dental and Medical Sciences* **2021,** *3,* 78–85, https://doi.org/10.30485/ijsrdms.2021.287932.1160.
52. Shangloo, P.; Gupte, B.; Syed, M. Histopathological effect of arsenic in drinking water on liver and kidney of albino rat: a light microscopic study. *International Journal of Scientific Research in Dental and Medical Sciences* **2021,** *3,* 166–170, https://doi.org/10.30485/ijsrdms.2021.313575.1213.
53. Petrovic, B.; Gorbounov, M.; Soltani, S.M. Influence of surface modification on selective CO2 adsorption: a technical review on mechanisms and methods. *Microporous and Mesoporous Materials* **2021,** *312,* 110751, https://doi.org/10.1016/j.micromeso.2020.110751.
54. Najafloo, A.; Sakhaeinia, H. Modeling the solubility of carbon dioxide in the MDEA+ AEEA aqueous solution using the SAFT-HR equation of state and extended UNIQUAC model. *Main Group Chemistry* **2022,** *21,* 1–17, https://doi.org/10.3233/mgc-210061.
55. Zarifi, K.; Rezaei, F.; Seyed Alizadeh, S.M. A mosdel of FeN-decorated BeO layer particle for CO gas adsorption. *Main Group Chemistry* **2022,** *21,* 125–132, https://doi.org/10.3233/mgc-210100.
56. Mollazehi, F. Catalytic nanoparticles and magnetic nanocatalysts in organic reactions: a mini review. *Main Group Chemistry* **2022,** *21,* 697–708, https://doi.org/10.3233/mgc-210170.
57. Frisch, M.J.; Trucks, G.W.; Schlegel, H.B. et al. Gaussian 09 program **2009**. *Gaussian Inc*. Wallingford, CT.
58. Wilson, T.R.; Alexandrova, A.N.; Eberhart, M.E. Electron density geometry and the quantum theory of atoms in molecules. *The Journal of Physical Chemistry A* **2021,** *125,* 10622–10631, https://doi.org/10.1021/acs.jpca.1c09359.
59. Koirala, M.; Alexov, E. Computational chemistry methods to investigate the effects caused by DNA variants linked with disease. *Journal of Theoretical and Computational Chemistry* **2020,** *19,* 1930001, https://doi.org/10.1142/S0219633619300015.
60. Venkatesh, G.; Sheena mary, Y.; Shymamary, Y.; Palanisamy, V.; Govindaraju, M. Quantum chemical and molecular docking studies of some phenothiazine derivatives. *Journal of Applied Organometallic Chemistry* **2021,** *1,* 148–158, https://doi.org/10.22034/jaoc.2021.303059.1033.
61. Rather, A.; Wani, G.M.; Robbani, I. Multidetector-row computed tomography and colour doppler imaging in the evaluation of patients with extrahepatic portal hypertension: a prospective study. *International Journal of Scientific Research in Dental and Medical Sciences* **2021,** *3,* 86–93, http://doi.org/10.30485/IJSRDMS.2021.285539.1153.
62. Rim, K.; Ameni, C.; Garrach, B.E.; Chaouch, M.H.; Touzi, S. Anatomical dimension of the anterior maxillary alveolar process: a cone beam computed tomography study. *International Journal of Scientific Research in Dental and Medical Sciences* **2021,** *3,* 111–116, https://doi.org/10.30485/ijsrdms.2021.289617.1167.
63. Farhami, N. A computational study of thiophene adsorption on boron nitride nanotube. *Journal of Applied Organometallic Chemistry* **2022,** *2,* 163–172, https://doi.org/10.22034/jaoc.2022.154821.